

# EFFECT OF MICROSTRUCTURE ON FIBER/MATRIX INTERFACE CRACK GROWTH IN UD AND CROSS-PLY LAMINATES UNDER TENSILE LOADING

## INSIGHTS FROM LINEAR ELASTIC FRACTURE MECHANICS

Luca Di Stasio<sup>1,2</sup>, Janis Varna<sup>1</sup>, Zoubir Ayadi<sup>2</sup>

<sup>1</sup> Division of Materials Science, Luleå University of Technology, Luleå, Sweden

<sup>2</sup>EEIGM & IJL, Université de Lorraine, Nancy, France

Grupo de Elasticidad y Resistencia de Materiales, ETSI Sevilla

Sevilla (ES) - September 26, 2019



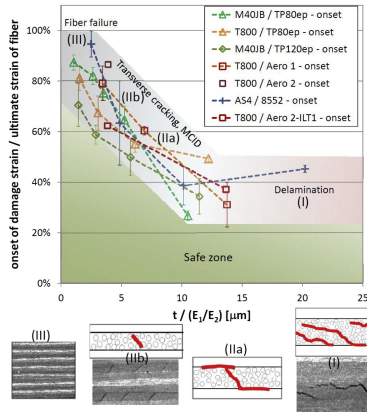
## Outline

- ➔ Transverse Cracks Initiation
- ➔ Modeling
- ➔ Convergence
- ➔ Debond Initiation
- ➔ Debond Propagation
- ➔ Moving Forward

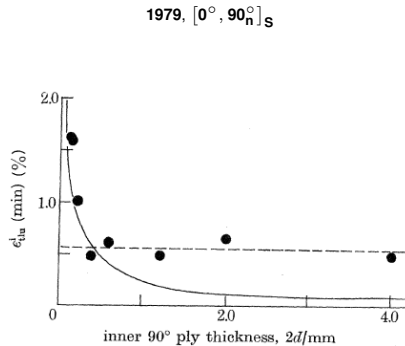
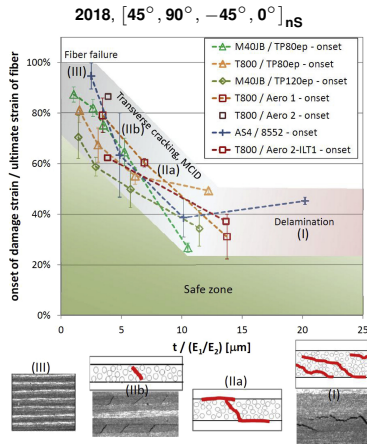
Transverse Cracks Initiation Modeling Convergence Debond Initiation Debond Propagation Moving Forward  
The Thin-ply "Advantage" Micromechanics of Initiation

## ➔ TRANSVERSE CRACKS INITIATION

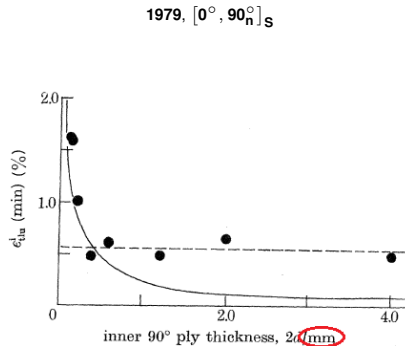
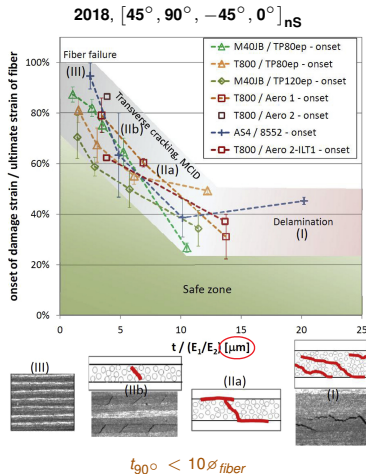
## The Thin-ply "Advantage": new material

2018,  $[45^\circ, 90^\circ, -45^\circ, 0^\circ]_{ns}$ Cugnoni et al., Compos. Sci. Technol. **168**, 2018.

## The Thin-ply "Advantage": new material, old result



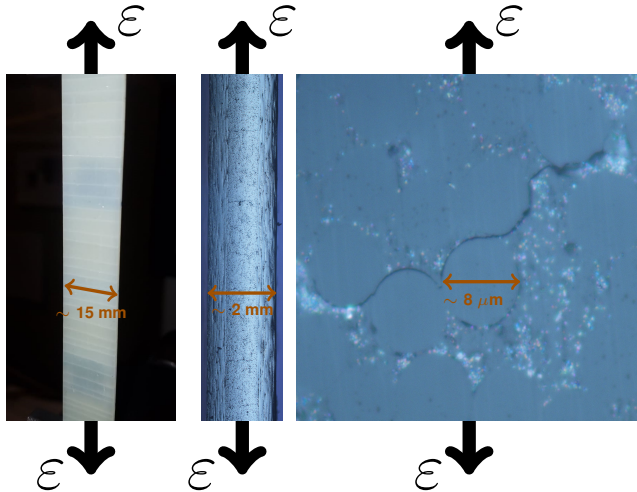
## The Thin-ply "Advantage": new material, old result?



Cugnoni et al., Compos. Sci. Technol. **168**, 2018.

Bailey et al., P. Roy. Soc. A-Math. Phys. **366** (1727), 1979.

## Micromechanics of Initiation



**Left:**  
front view of [0, 90<sub>2</sub>]<sub>S</sub>,  
visual inspection.

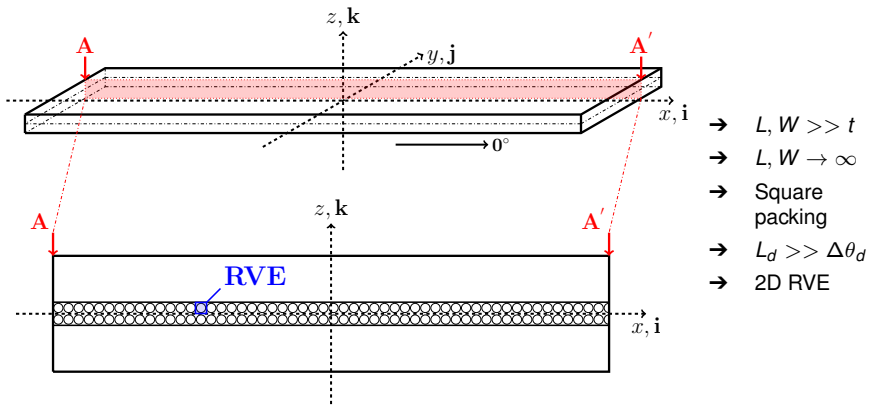
**Center:**  
edge view of [0, 90]<sub>S</sub>,  
optical microscope.

**Right:**  
edge view of [0, 90]<sub>S</sub>,  
optical microscope.

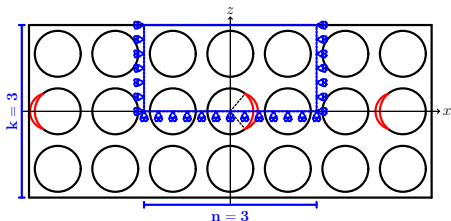
Transverse Cracks Initiation Modeling Convergence Debond Initiation Debond Propagation Moving Forward  
Geometry Representative Volume Elements Equivalent boundary conditions Assumptions Solution

## **MODELING**

## Geometry

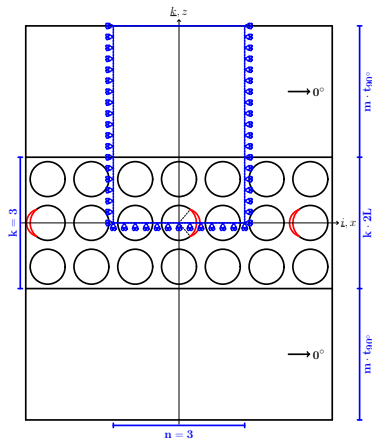


## Representative Volume Elements



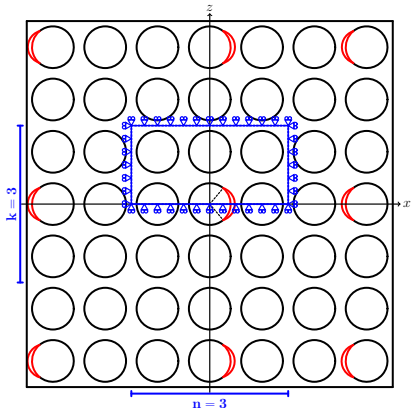
$n \times k - \text{free}$

$n \times k - H$



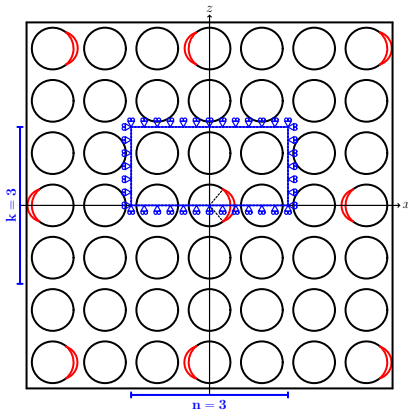
$n \times k - m \cdot t_{90^\circ}$

## Representative Volume Elements



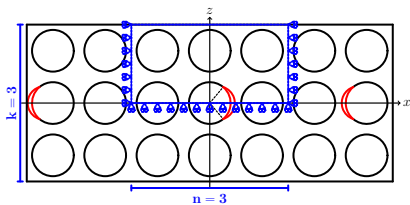
$n \times k - \text{symm (coupling)}$

$n \times k - \text{coupling} + H$



$n \times k - \text{asymm}$

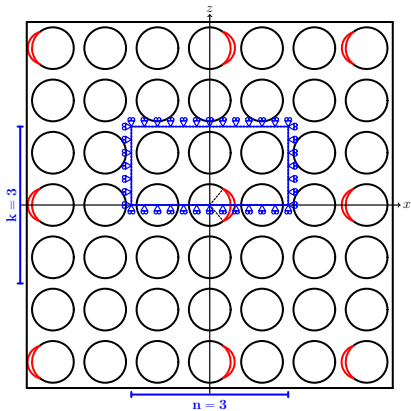
## Equivalent boundary conditions: linear horizontal displacement ( $H$ )



$$u_x(x, h) = \bar{\varepsilon}_x x$$

$$n \times k - H$$

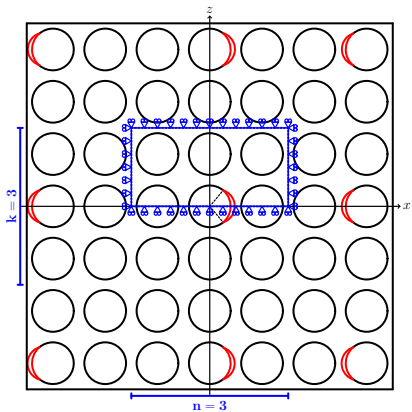
## Equivalent boundary conditions: symmetric coupling



$$u_z(x, h) = \bar{u}_z(x, h)$$

$n \times k - \text{symm (coupling)}$

## Equivalent boundary conditions: coupling + H



$$u_z(x, h) = \bar{u}_z(x, h)$$

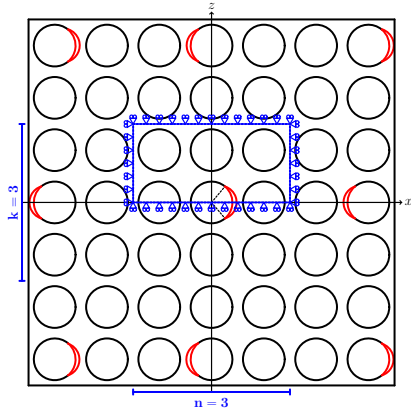
$$u_x(x, h) = \bar{\varepsilon}_x x$$

$n \times k - \text{coupling} + H$

## Equivalent boundary conditions: anti-symmetric coupling

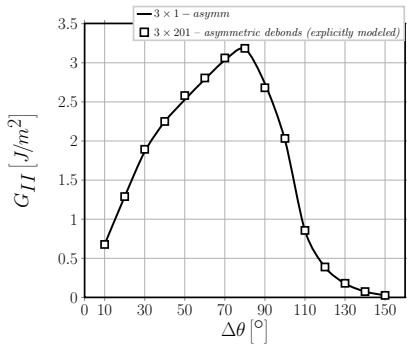
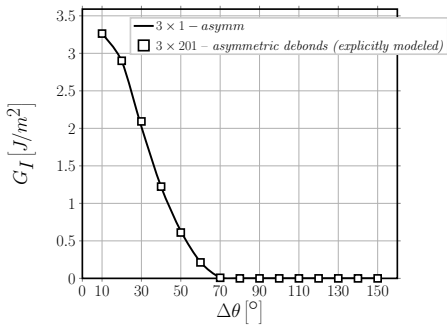
$$u_z(x, h) = -u_z(0, h) = \\ - (u_z(-x, h) - u_z(0, h))$$

$$u_x(x, h) = -u_x(-x, h)$$

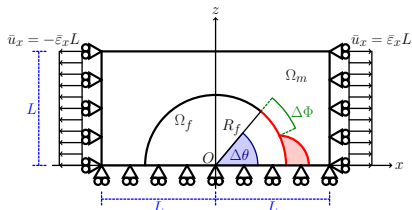


$n \times k - \text{asym}$

## Equivalent boundary conditions: validation



## Assumptions

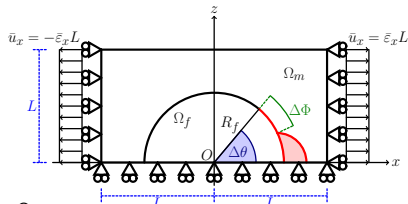


$$R_f = 1 \text{ } [\mu\text{m}] \quad L = \frac{R_f}{2} \sqrt{\frac{\pi}{V_f}}$$

- Linear elastic, homogeneous materials
- Concentric Cylinders Assembly with Self-Consistent Shear Model for UD
- Plane strain
- Frictionless contact interaction
- Symmetric w.r.t. x-axis
- Coupling of x-displacements on left and right side (repeating unit cell)
- Applied uniaxial tensile strain  $\bar{\epsilon}_x = 1\%$
- $V_f = 60\%$

Material	$V_f$ [%]	$E_L$ [GPa]	$E_T$ [GPa]	$\mu_{LT}$ [GPa]	$\nu_{LT}$ [-]	$\nu_{TT}$ [-]
Glass fiber	-	70.0	70.0	29.2	0.2	0.2
Epoxy	-	3.5	3.5	1.25	0.4	0.4
UD	60.0	43.442	13.714	4.315	0.273	0.465

## Solution



in  $\Omega_f, \Omega_m, \Omega_{UD}$  :

$$\frac{\partial^2 \varepsilon_{xx}}{\partial z^2} + \frac{\partial^2 \varepsilon_{zz}}{\partial x^2} = \frac{\partial^2 \gamma_{zx}}{\partial x \partial z} \quad \text{for } 0^\circ \leq \alpha \leq \Delta\theta : \quad (\vec{u}_m(R_f, \alpha) - \vec{u}_f(R_f, \alpha)) \cdot \vec{n}_\alpha \geq 0$$

$$\varepsilon_y = \gamma_{xy} = \gamma_{yz} = 0$$

for  $\Delta\theta \leq \alpha \leq 180^\circ$  :

$$\frac{\partial \sigma_{xx}}{\partial x} + \frac{\partial \tau_{zx}}{\partial z} = 0$$

$$\vec{u}_m(R_f, \alpha) - \vec{u}_f(R_f, \alpha) = 0$$

$$\frac{\partial \tau_{zx}}{\partial x} + \frac{\partial \sigma_{zz}}{\partial z} = 0$$

$$\sigma_{ij} = E_{ijkl} \varepsilon_{kl}$$

+ BC

$$\sigma_{yy} = \nu (\sigma_{xx} + \sigma_{zz})$$

$\forall \Delta\theta \neq 0^\circ$

→ oscillating singularity

$$\sigma \sim r^{-\frac{1}{2}} \sin(\varepsilon \log r), \quad V_f \rightarrow 0$$

$$\varepsilon = \frac{1}{2\pi} \log \left( \frac{1-\beta}{1+\beta} \right)$$

$$\beta = \frac{\mu_2(\kappa_1 - 1) - \mu_1(\kappa_2 - 1)}{\mu_2(\kappa_1 + 1) + \mu_1(\kappa_2 + 1)}$$

→ receding contact

$$\rightarrow \frac{G(R_{f,2})}{G(R_{f,1})} = \frac{R_{f,2}}{R_{f,1}}, \quad \frac{G(\bar{\varepsilon}_{x,2})}{G(\bar{\varepsilon}_{x,1})} = \frac{\bar{\varepsilon}_{x,2}^2}{\bar{\varepsilon}_{x,1}^2}$$

→ FEM + LEFM (VCCT)

→ regular mesh of quadrilaterals at the crack tip:

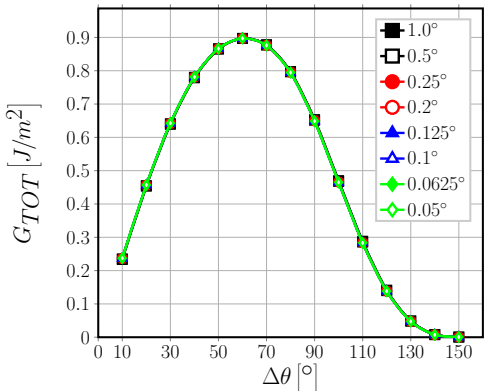
$$- \quad AR \sim 1, \quad \delta = 0.05^\circ$$

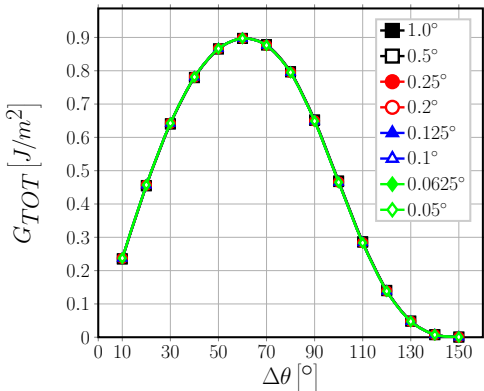
$\forall \Delta\theta$

→ 2<sup>nd</sup> order shape functions

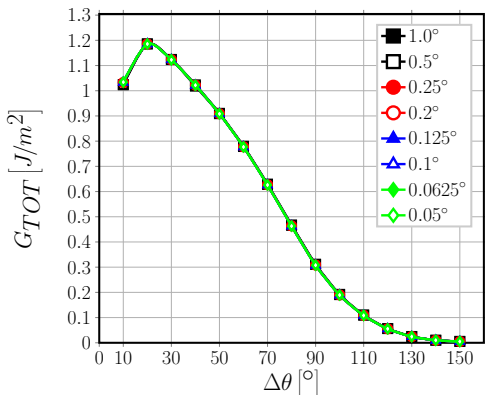
Transverse Cracks Initiation Modeling Convergence Debond Initiation Debond Propagation Moving Forward  
 $G_{TOT}$   $G_I$   $G_{II}$  Vectorial formulation of VCCT Asymptotic behavior Numerical convergence  $\delta$  selection

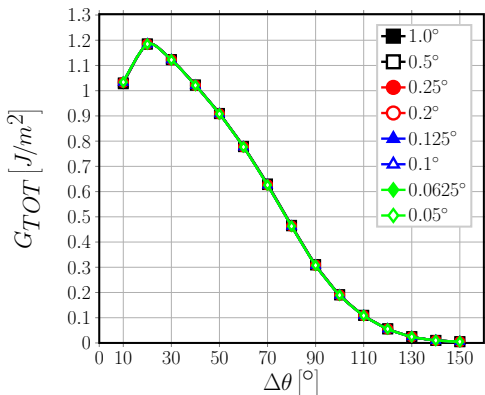
# CONVERGENCE

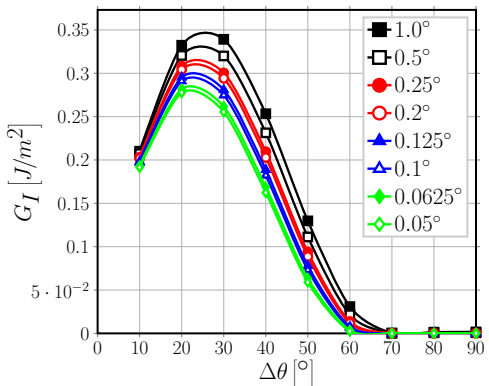
$G_{TOT}$  $\rightarrow 1 \times 1 - free, V_f = 0.1\%, 1^{st} \text{ order elements}$

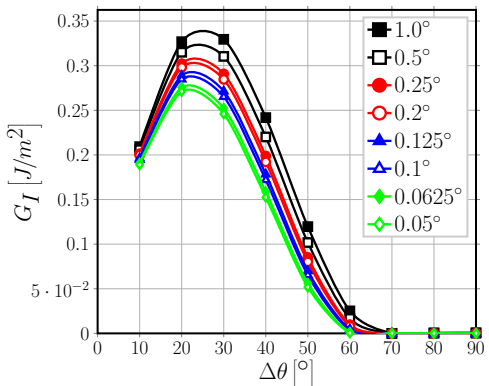
$G_{TOT}$ 

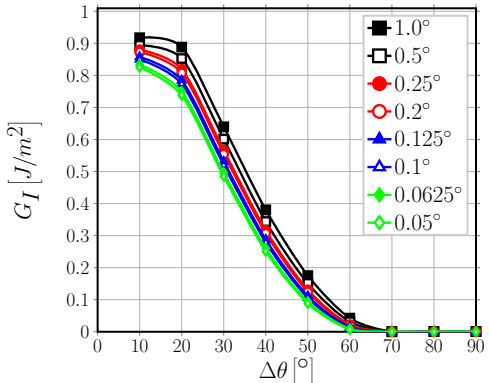
$\rightarrow 1 \times 1 - free, V_f = 0.1\%, 2^{nd} order elements$

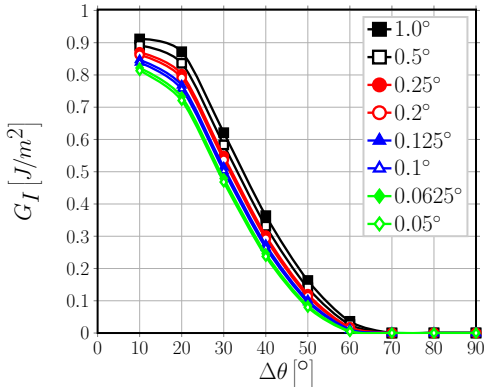
$G_{TOT}$  $\rightarrow 1 \times 1 - free, V_f = 40\%, 1^{st} order elements$

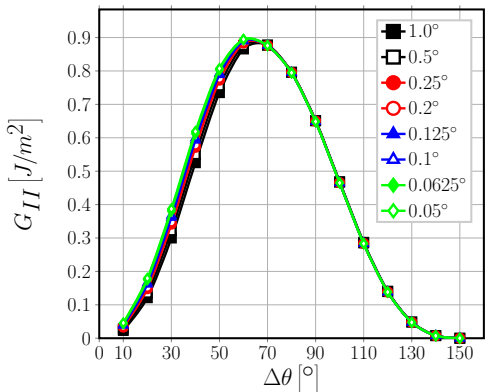
$G_{TOT}$  $\rightarrow 1 \times 1 - free, V_f = 40\%, 2^{nd} order elements$

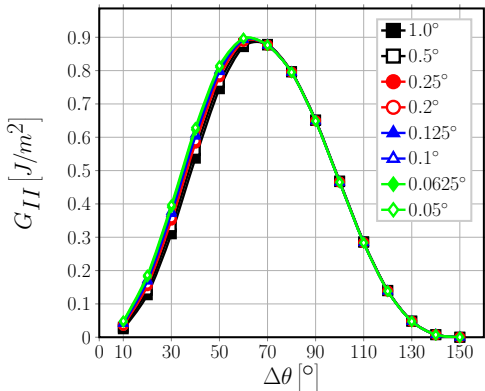
$G_I$  $\rightarrow 1 \times 1 - free, V_f = 0.1\%, 1^{st} \text{ order elements}$

$G_I$  $\rightarrow 1 \times 1 - free, V_f = 0.1\%, 2^{nd} \text{ order elements}$

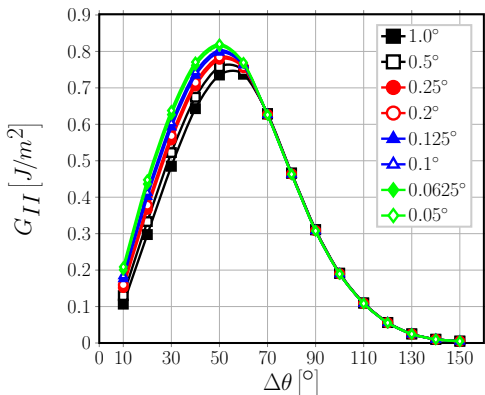
$G_I$  $\rightarrow 1 \times 1 - free, V_f = 40\%, 1^{st} order elements$

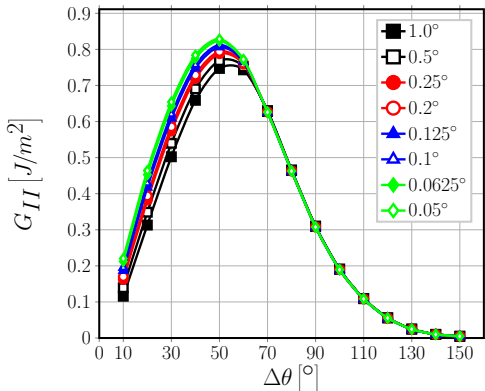
$G_I$  $\rightarrow 1 \times 1 - free, V_f = 40\%, 2^{nd} \text{ order elements}$

$G_{II}$  $\rightarrow 1 \times 1 - free, V_f = 0.1\%, 1^{st} \text{ order elements}$

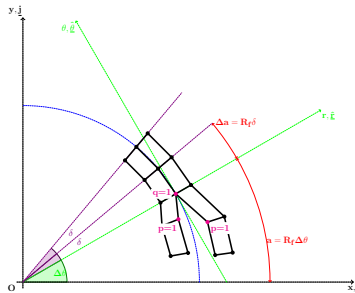
$G_{II}$ 

$\rightarrow 1 \times 1 - free, V_f = 0.1\%, 2^{nd} \text{ order elements}$

$G_{II}$  $\rightarrow 1 \times 1 - free, V_f = 40\%, 1^{st} order elements$

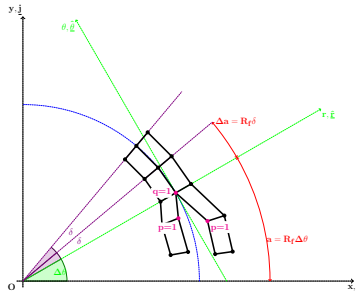
$G_{II}$  $\rightarrow 1 \times 1 - free, V_f = 40\%, 2^{nd} \text{ order elements}$

## Vectorial formulation of VCCT



$$\begin{aligned}
 G_{TOT} = & \frac{1}{2R_f\delta} \sum_{p=1}^{m+1} \sum_{q=1}^{m+1} \text{Tr} \left( Q \underline{\underline{R}}_{\underline{\underline{\delta}}=\Delta\theta} \underline{\underline{K}}_{xy,q} \underline{\underline{u}}_{xy,q}^T \underline{\underline{u}}_{xy,p} \underline{\underline{R}}_{\underline{\underline{\Delta\theta}}=\delta}^T \underline{\underline{P}}_{pq}^T \underline{\underline{T}}_{pq}^T \right) + \\
 & + \frac{1}{2R_f\delta} \sum_{p=1}^{m+1} \sum_{q=1}^{m+1} \text{Tr} \left( Q \underline{\underline{R}}_{\underline{\underline{\Delta\theta}}=\Delta\theta} \widetilde{\underline{\underline{F}}}_{xy,q} \underline{\underline{u}}_{xy,p}^T \underline{\underline{R}}_{\underline{\underline{\Delta\theta}}=\delta}^T \underline{\underline{P}}_{pq}^T \underline{\underline{T}}_{pq}^T \right)
 \end{aligned}$$

## Vectorial formulation of VCCT



$$\underline{G} = \begin{bmatrix} G_I \\ G_{II} \end{bmatrix} = \frac{1}{2R_f\delta} \sum_{p=1}^{m+1} \sum_{q=1}^{m+1} Diag \left( Q_{\underline{\delta}=\Delta\theta} R_{\underline{\Delta\theta}=\Delta\theta, q} K_{\underline{xy}, q} u_{xy, q}^T u_{xy, p}^T R_{\underline{\Delta\theta}=\delta}^T P_{\underline{\delta}=\delta}^T T_{pq}^T \right) + \\ + \frac{1}{2R_f\delta} \sum_{p=1}^{m+1} \sum_{q=1}^{m+1} Diag \left( Q_{\underline{\delta}=\Delta\theta} R_{\underline{\Delta\theta}=\Delta\theta, q} \tilde{K}_{\underline{N}, q} u_N^T u_{xy, p}^T R_{\underline{\Delta\theta}=\delta}^T P_{\underline{\delta}=\delta}^T T_{pq}^T \right)$$

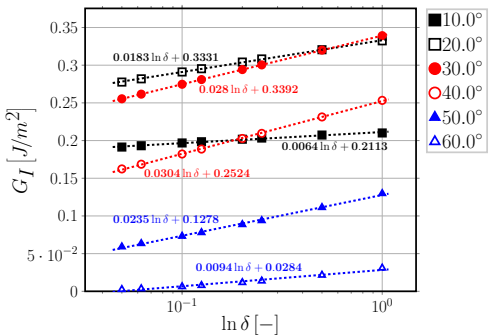
## Asymptotic behavior

$$\frac{\partial \underline{G}}{\partial \delta} = \frac{1}{\delta} \underline{G} + \frac{1}{2R_f \delta} (\dots)$$

$$u(\delta) \sim \sqrt{\delta} (\sin, \cos)(\epsilon \log \delta) \quad \text{with} \quad \epsilon = \frac{1}{2\pi} \log \left( \frac{1-\beta}{1+\beta} \right)$$

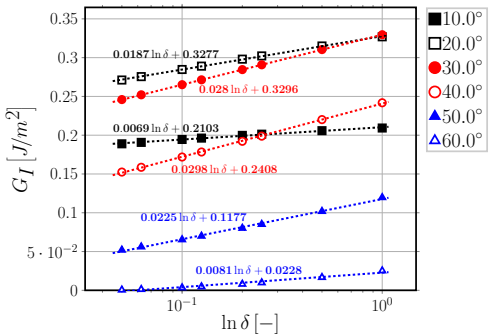
$$\lim_{\delta \rightarrow 0} \frac{\partial \underline{G}}{\partial \delta} \sim \frac{1}{\delta} \xrightarrow{\int d\delta} \lim_{\delta \rightarrow 0} \underline{G} \sim \underline{A} \log(\delta) + \underline{B}.$$

## Numerical convergence: $G_I$



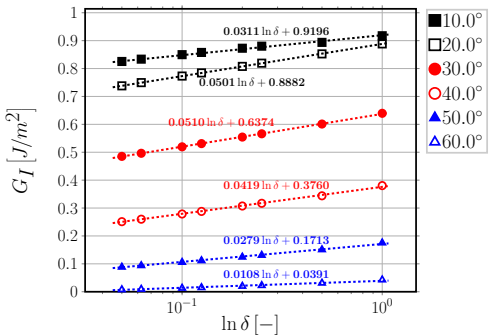
$\rightarrow 1 \times 1 - \text{free}, V_f = 0.1\%, 1^{\text{st}} \text{ order elements}$

## Numerical convergence: $G_I$



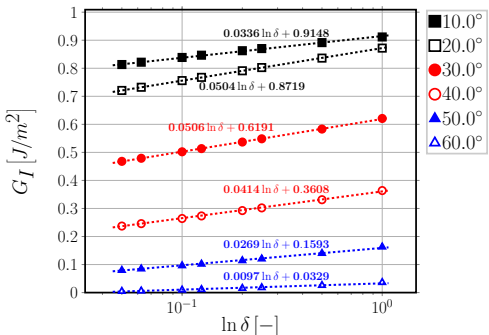
$\rightarrow 1 \times 1 - \text{free}, V_f = 0.1\%, 2^{\text{nd}} \text{ order elements}$

## Numerical convergence: $G_I$



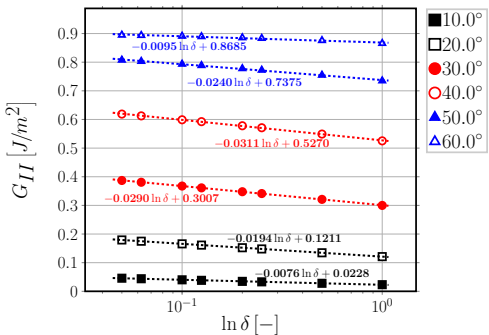
$\rightarrow 1 \times 1 - free, V_f = 40\%, 1^{st} order elements$

## Numerical convergence: $G_I$



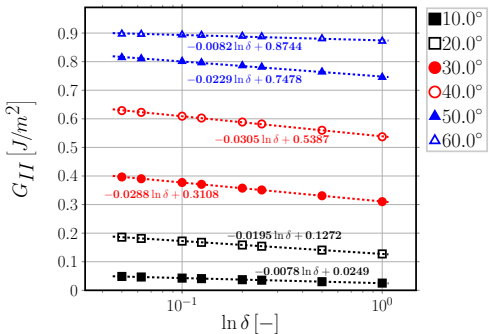
$\rightarrow 1 \times 1 - free, V_f = 40\%, 2^{nd} \text{ order elements}$

## Numerical convergence: $G_{II}$



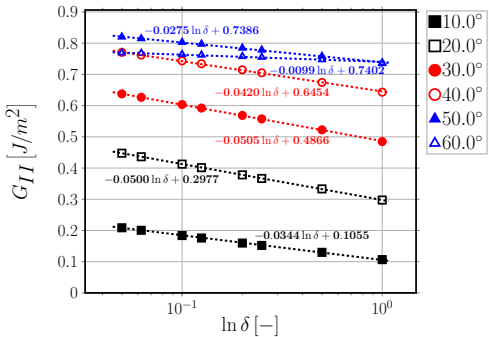
$\rightarrow 1 \times 1 - free, V_f = 0.1\%, 1^{st} order elements$

## Numerical convergence: $G_{II}$



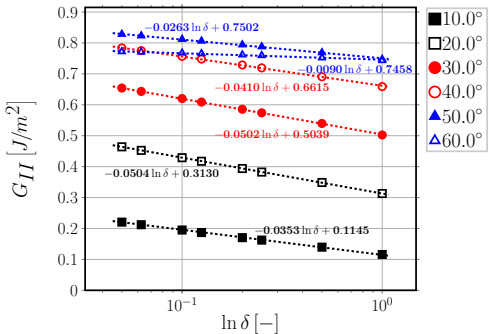
→ 1 × 1 – free,  $V_f = 0.1\%$ , 2<sup>nd</sup> order elements

## Numerical convergence: $G_{II}$



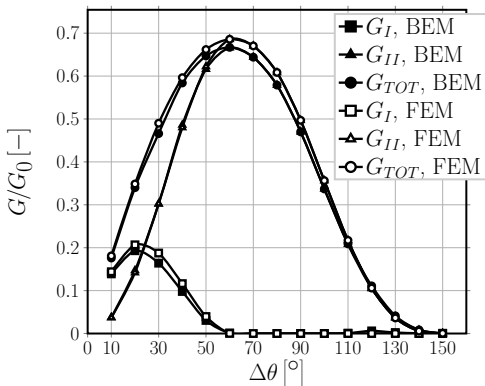
$\rightarrow 1 \times 1 - free, V_f = 40\%, 1^{st} order elements$

## Numerical convergence: $G_{II}$



$\rightarrow 1 \times 1 - free, V_f = 40\%, 2^{nd} order elements$

## $\delta$ selection

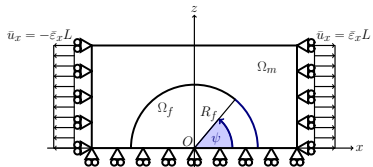
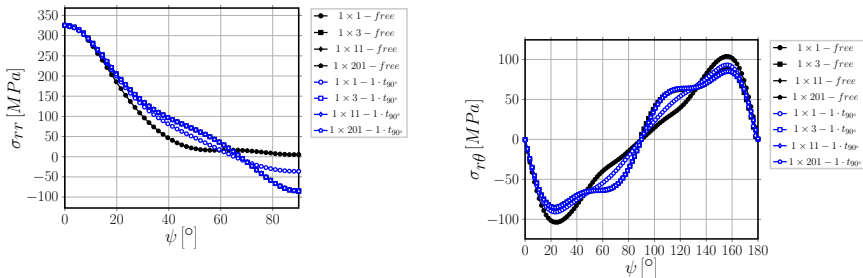


$\rightarrow 1 \times 1 - \text{free}, V_f = 0.01\%, 2^{\text{nd}} \text{ order elements}, \delta = 0.05^\circ$

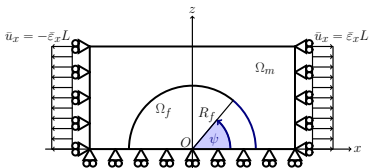
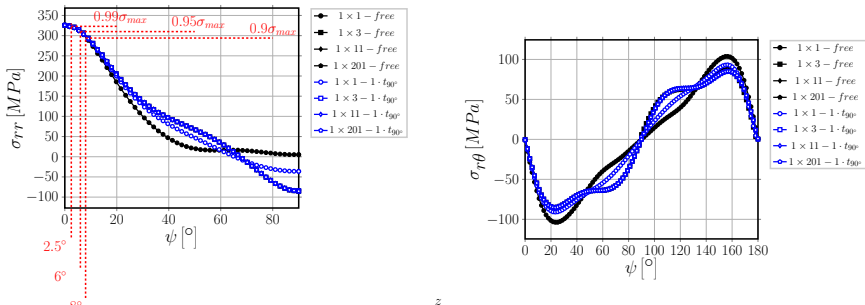
Transverse Cracks Initiation Modeling Convergence Debond Initiation Debond Propagation Moving Forward  
 $\sigma_{rr}$  vs  $\tau_{r\theta}$   $\sigma_{LHS}$   $\sigma_{vM}$   $\sigma_I$  Observations

## DEBOND INITIATION

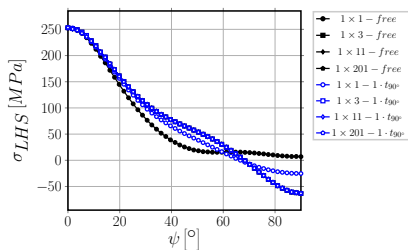
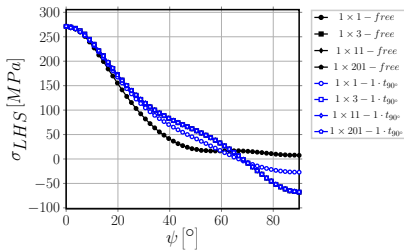
## $\sigma_{rr}$ vs $\tau_{r\theta}$ : radial stress vs tangential shear at the interface



## $\sigma_{rr}$ vs $\tau_{r\theta}$ : radial stress vs tangential shear at the interface

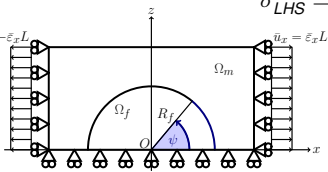


## $\sigma_{LHS}$ : local hydrostatic stress at the interface

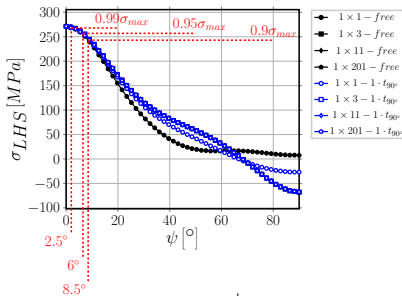


$$\sigma_{LHS}^{2D} = \frac{\sigma_{rr} + \sigma_{\theta\theta}}{2}$$

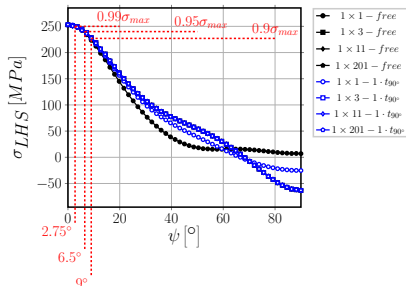
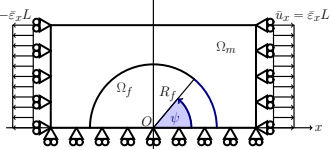
$$\sigma_{LHS}^{3D} = \frac{\sigma_{rr} + \sigma_{\theta\theta} + \sigma_{yy}}{3}$$



## $\sigma_{LHS}$ : local hydrostatic stress at the interface

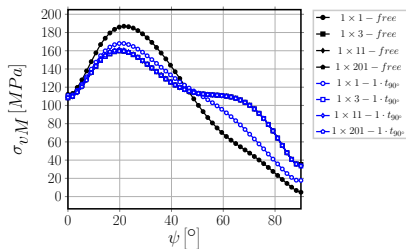
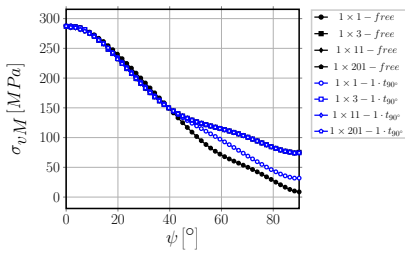


$$\sigma_{LHS}^{2D} = \frac{\sigma_{rr} + \sigma_{\theta\theta}}{2}$$



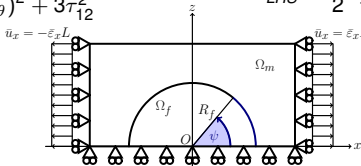
$$\sigma_{LHS}^{3D} = \frac{\sigma_{rr} + \sigma_{\theta\theta} + \sigma_{yy}}{3}$$

## $\sigma_{vM}$ : von Mises stress at the interface

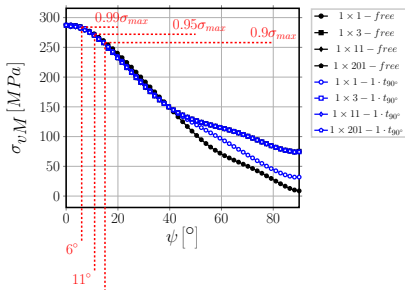


$$\sigma_{vM}^{2D} = \sqrt{(\sigma_{rr} - \sigma_{\theta\theta})^2 + 3\tau_{12}^2}$$

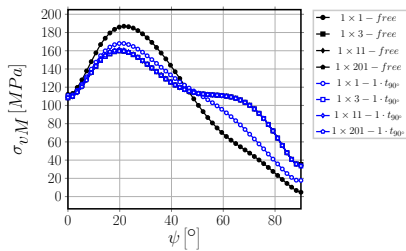
$$\sigma_{LHS}^{3D} = \frac{3}{2} s_{ij} s_{ij} \quad s_{ij} = \sigma_{ij} - \frac{1}{3} \sigma_{kk} \delta_{ij}$$



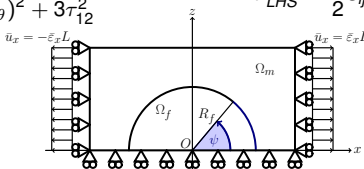
## $\sigma_{vM}$ : von Mises stress at the interface



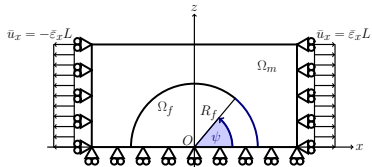
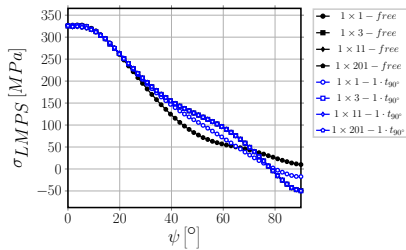
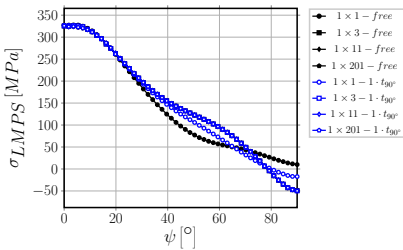
$$\sigma_{vM}^{2D} = \sqrt{(\sigma_{rr} - \sigma_{\theta\theta})^2 + 3\tau_{12}^2}$$



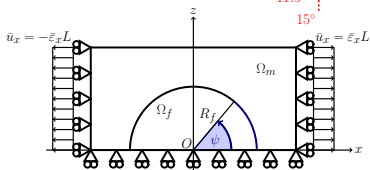
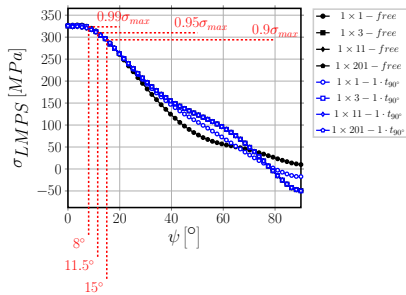
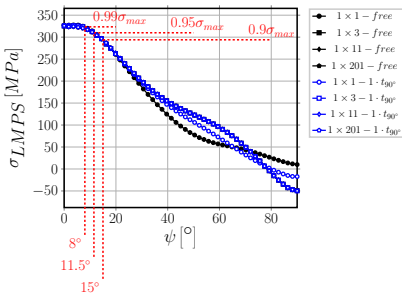
$$\sigma_{LHS}^{3D} = \frac{3}{2} s_{ij} s_{ij} \quad s_{ij} = \sigma_{ij} - \frac{1}{3} \sigma_{kk} \delta_{ij}$$



## $\sigma_I$ : maximum principal stress at the interface



## $\sigma_I$ : maximum principal stress at the interface



## Observations

- For all stresses analyzed, no significant difference is present between the different RUCs for  $\psi \leq 10^\circ$ ;
- for all stresses analyzed, no difference can be observed by increasing  $k$  when  $k \geq 3$ ;
- for all stresses analyzed, no difference can be observed between  $1 \times k - \text{free}$  and  $1 \times k - 1 \cdot t_{90^\circ}$  for  $k \geq 3$ ;
- $\sigma_{rr}$ ,  $\sigma_{LHS,2D}$ ,  $\sigma_{LHS,3D}$ ,  $\sigma_{vM,2D}$ ,  $\sigma_{LMPS,2D}$  and  $\sigma_{LMPS,3D}$  all reach their peak value at  $0^\circ$  and  $180^\circ$  and decrease to 99% the peak value between  $2^\circ$  and  $8^\circ$ , to 95% the peak value between  $6^\circ$  and  $12^\circ$  and to 90% the peak value between  $8^\circ$  and  $15^\circ$  from the occurrence of the maximum.

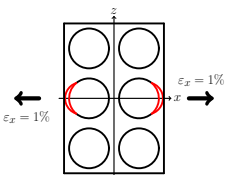
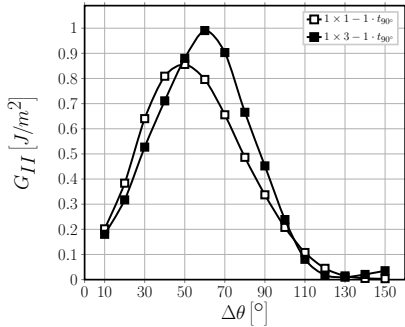
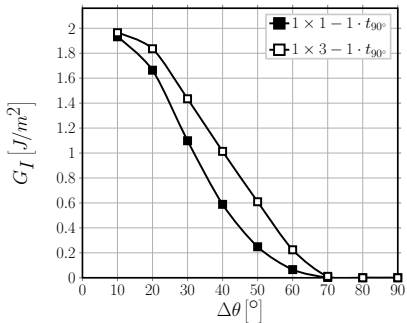
**It seems reasonable to conclude that...**

...a stress-based criterion would predict, irrespectively of the specific criterion chosen, the onset of an interface crack at  $0^\circ$  or  $180^\circ$  with an initial size at least comprised in the range  $2^\circ - 8^\circ$  (1% margin) and likely in the range  $6^\circ - 12^\circ$  (5% margin). Thus, no evident effect of  $90^\circ$  or  $0^\circ$  layer thickness can be observed.

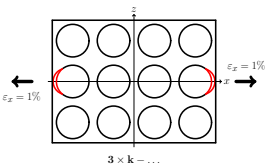
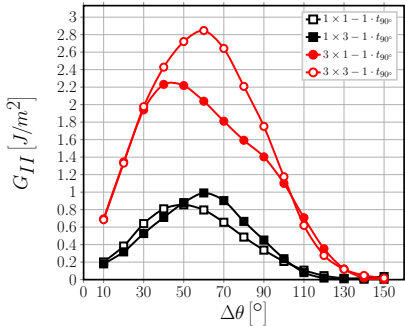
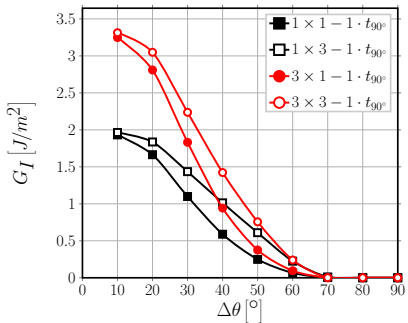
Transverse Cracks Initiation Modeling Convergence Debond Initiation Debond Propagation Moving Forward  
Debond Interaction: Horizontal Debond Interaction: Vertical  $0^\circ$  ply thickness  $90^\circ$  ply thickness  $G_{Ic}$   $\Delta\theta_{max}$  Comparison

# DEBOND PROPAGATION

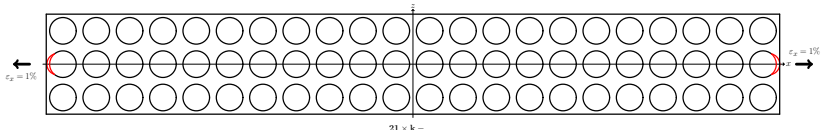
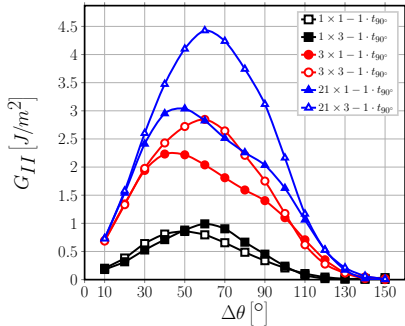
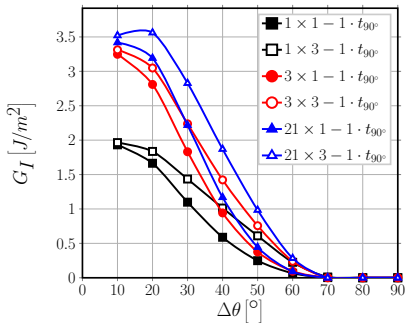
## Interaction of Debonds: Strain Magnification



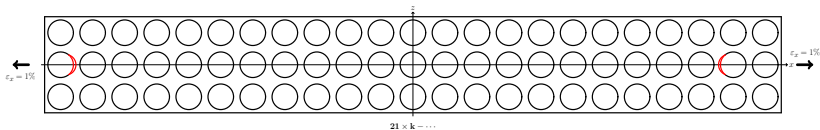
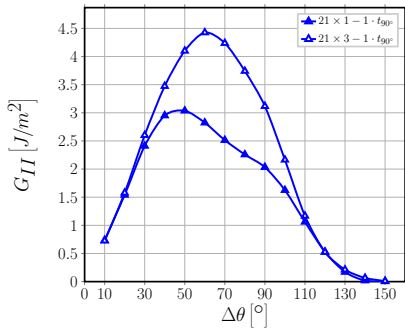
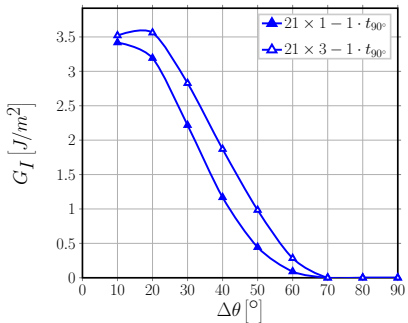
## Interaction of Debonds: Strain Magnification



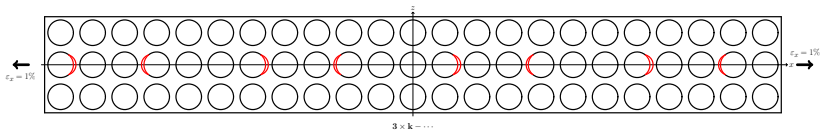
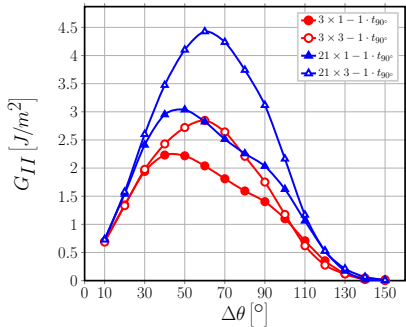
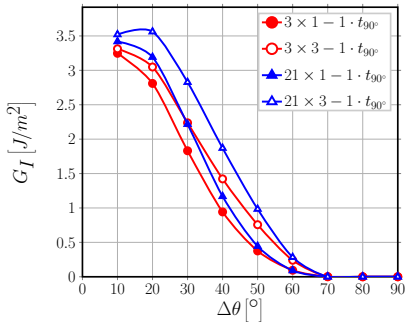
## Interaction of Debonds: Strain Magnification



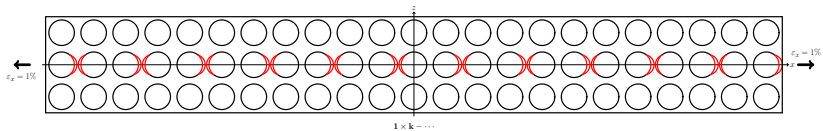
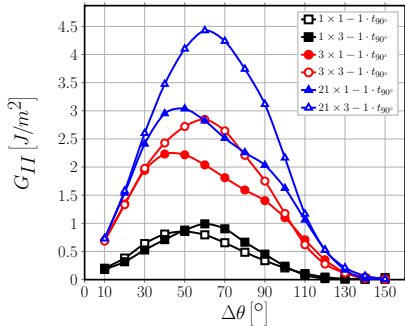
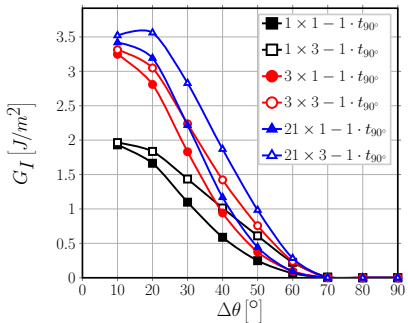
## Interaction of Debonds: Crack Shielding



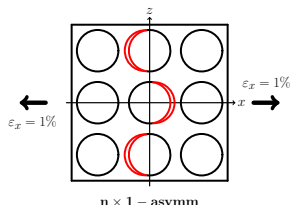
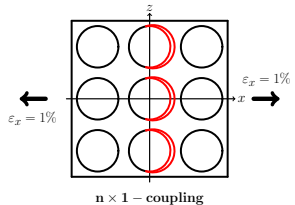
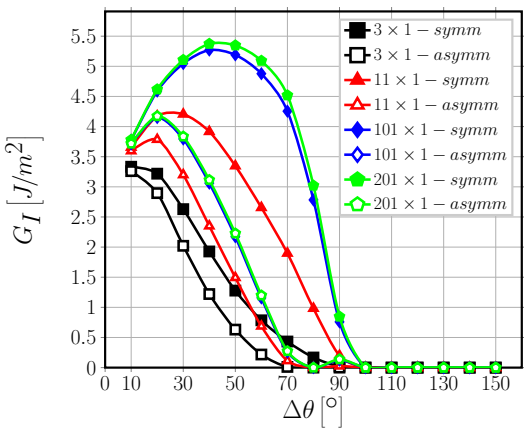
## Interaction of Debonds: Crack Shielding



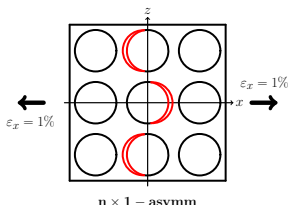
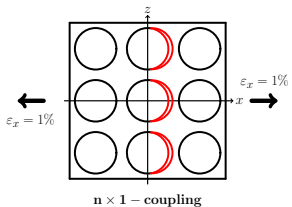
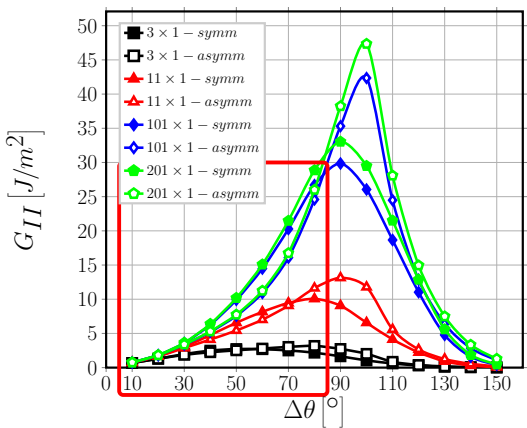
## Interaction of Debonds: Crack Shielding



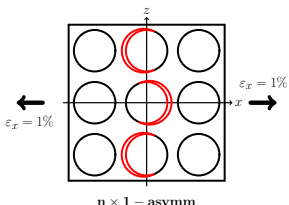
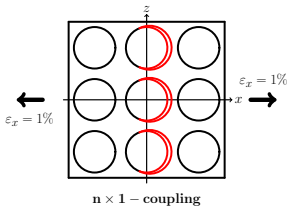
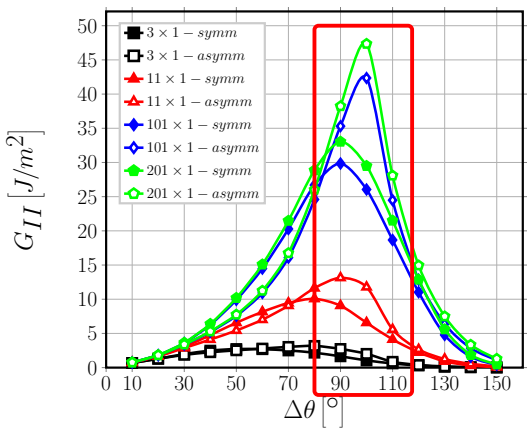
## Consecutive Debonds: Mode I



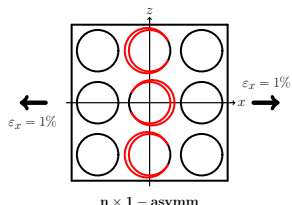
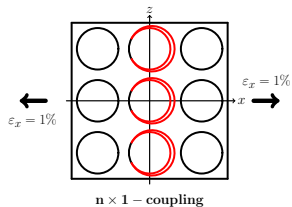
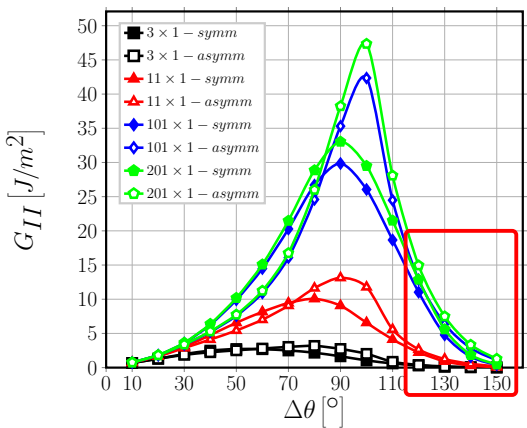
## Consecutive Debonds: Mode II



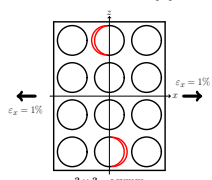
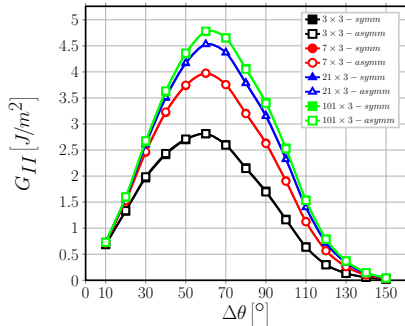
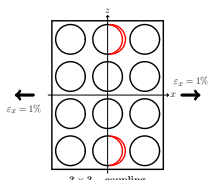
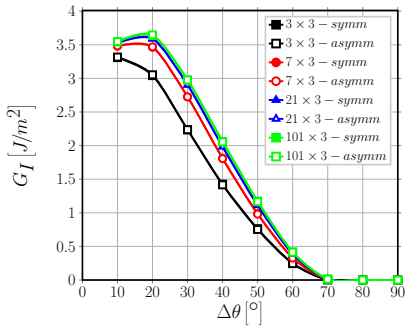
## Consecutive Debonds: Mode II



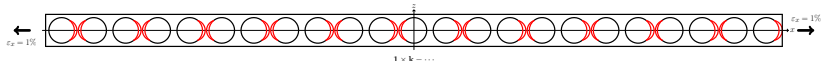
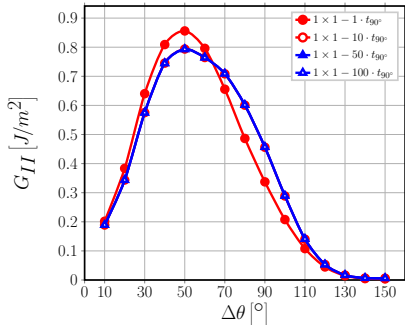
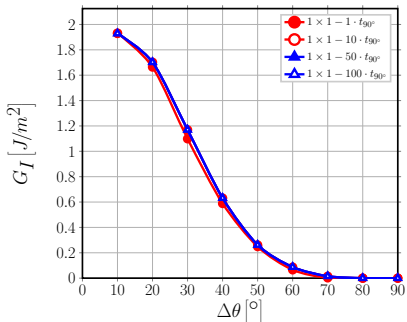
## Consecutive Debonds: Mode II



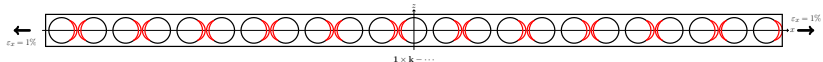
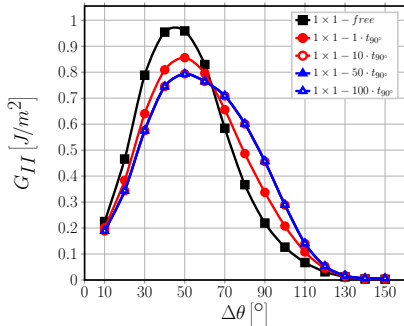
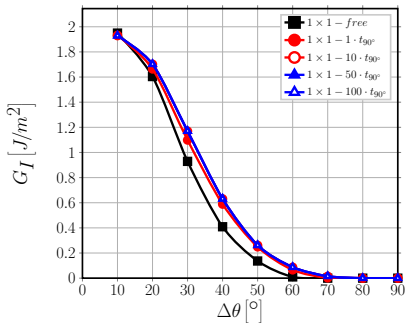
## Non-Consecutive Debonds



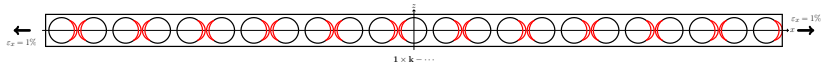
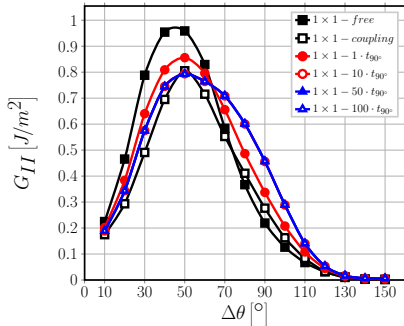
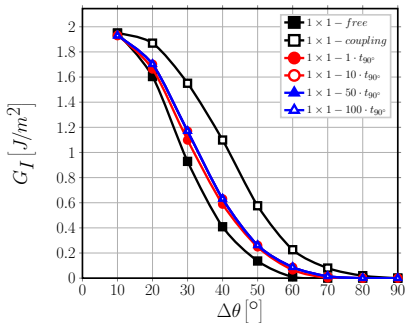
## Effect of $0^\circ$ ply thickness



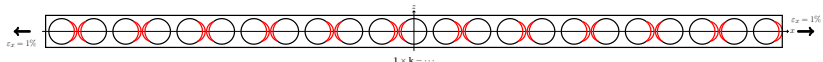
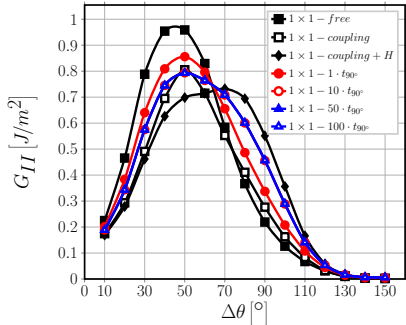
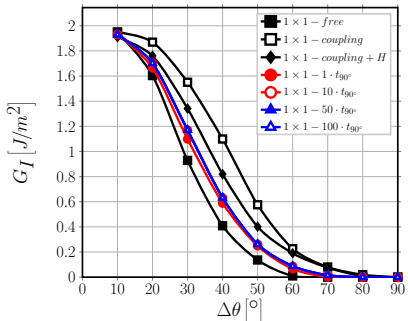
## Effect of $0^\circ$ ply thickness



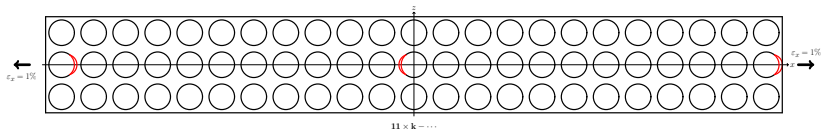
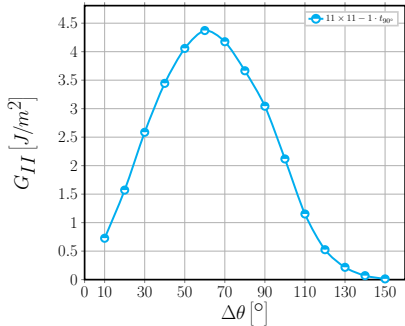
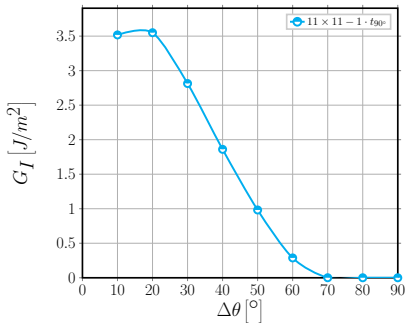
## Effect of $0^\circ$ ply thickness



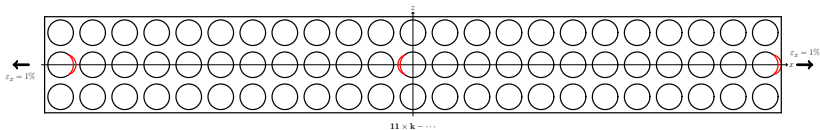
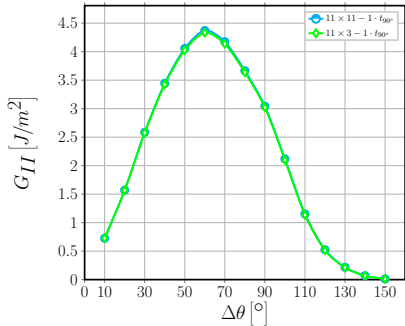
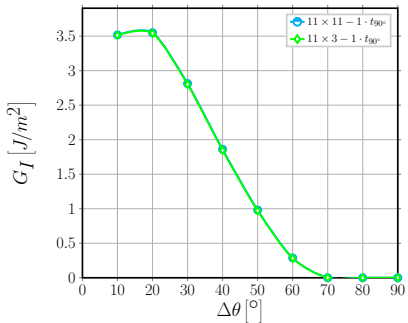
## Effect of $0^\circ$ ply thickness



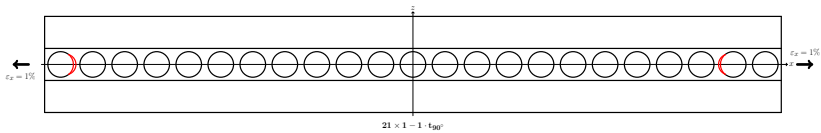
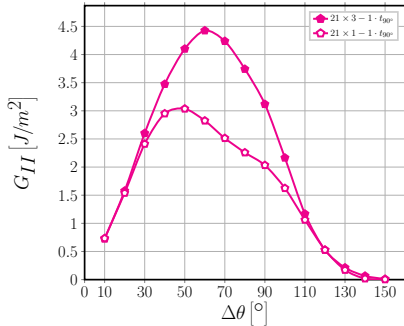
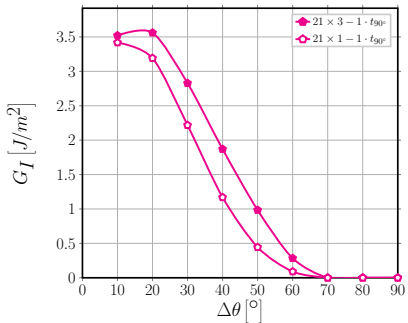
## Effect of $90^\circ$ ply thickness



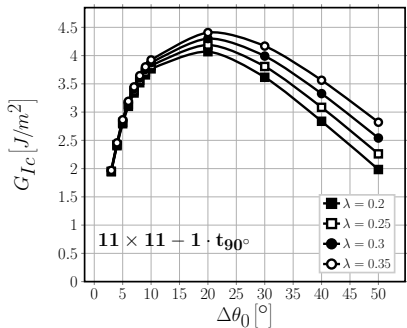
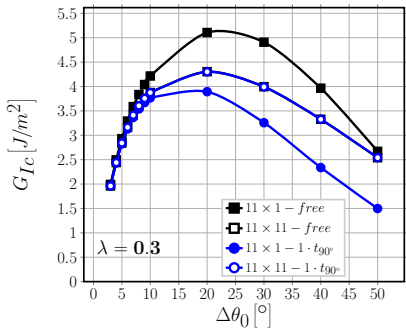
## Effect of $90^\circ$ ply thickness



## Effect of $90^\circ$ ply thickness



## Estimation of $G_{Ic}$

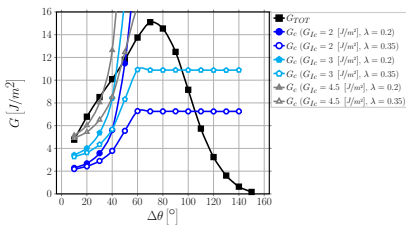


$$G_{Ic} = \frac{G_c}{1 + \tan^2((1 - \lambda) \Psi_G)} \Big|_{G_c=G_{TOT}(\Delta\theta_0)}, \quad \Psi_G = \tan^{-1} \left( \sqrt{\frac{G_{II}}{G_I}} \right) \Big|_{\Delta\theta_0}$$

$G_{Ic} \in [2, 4.5] \text{ J/m}^2$  with  $R_f = 1 \mu\text{m}$ ,  $\bar{\varepsilon}_x = 1\%$ ,  $G_{Ic} \in [3.2, 7.2] \text{ J/m}^2$  with  $R_f = 10 \mu\text{m}$ ,  $\bar{\varepsilon}_x = 0.4\%$

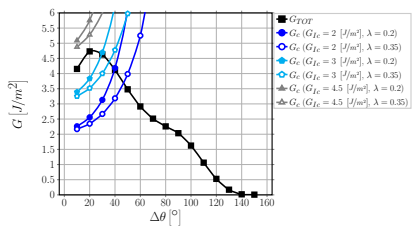
## Estimation of $\Delta\theta_{max}$

$21 \times 1 - free$



$$\Delta\theta_{max} \in (30^\circ - 105^\circ)$$

$21 \times 1 - 1 \cdot t_{90^\circ}$

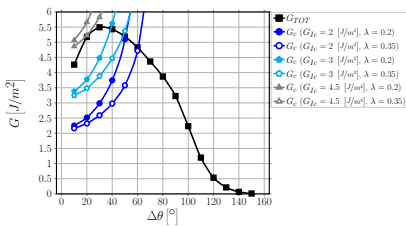


$$\Delta\theta_{max} \in (30^\circ - 50^\circ)$$

$$G_{TOT}(\Delta\theta) > G_c = G_{Ic} \left( 1 + \tan^2((1 - \lambda)\Psi_G) \right), \quad \Psi_G = \tan^{-1} \left( \sqrt{\frac{G_{II}}{G_I}} \right) \Big|_{\Delta\theta}$$

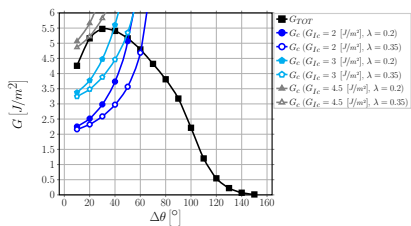
## Estimation of $\Delta\theta_{max}$

$21 \times 3 - free$



$\Delta\theta_{max} \in (40^\circ - 60^\circ)$

$21 \times 3 - 1 \cdot t_{90^\circ}$

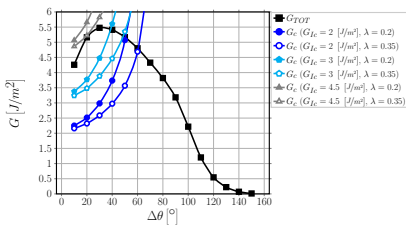


$\Delta\theta_{max} \in (40^\circ - 60^\circ)$

$$G_{TOT}(\Delta\theta) > G_c = G_{Ic} \left( 1 + \tan^2((1-\lambda)\Psi_G) \right), \quad \Psi_G = \tan^{-1} \left( \sqrt{\frac{G_{II}}{G_I}} \right) \Big|_{\Delta\theta}$$

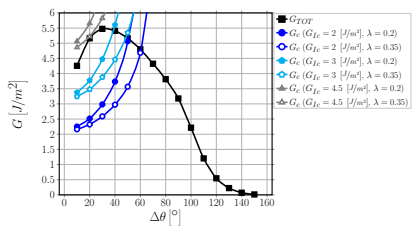
## Estimation of $\Delta\theta_{max}$

$21 \times 21 - free$



$\Delta\theta_{max} \in (40^\circ - 60^\circ)$

$21 \times 21 - 1 \cdot t_{90^\circ}$

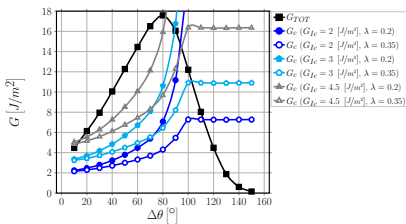


$\Delta\theta_{max} \in (40^\circ - 60^\circ)$

$$G_{TOT}(\Delta\theta) > G_c = G_{Ic} \left( 1 + \tan^2((1-\lambda)\Psi_G) \right), \quad \Psi_G = \tan^{-1} \left( \sqrt{\frac{G_{II}}{G_I}} \right) \Big|_{\Delta\theta}$$

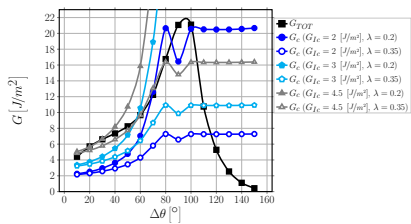
## Estimation of $\Delta\theta_{max}$

$21 \times 21 - symm$



$$\Delta\theta_{max} \in (80^\circ - 110^\circ)$$

$21 \times 21 - asymm$



$$\Delta\theta_{max} \in (55^\circ - 115^\circ)$$

$$G_{TOT}(\Delta\theta) > G_c = G_{lc} \left( 1 + \tan^2((1-\lambda)\Psi_G) \right), \quad \Psi_G = \tan^{-1} \left( \sqrt{\frac{G_{II}}{G_I}} \right) \Big|_{\Delta\theta}$$

## Comparison with Experimental Observations (literature)

Estimated debond size range in cross-ply ( $n \times k - 1 \cdot t_{90^\circ}$ )

$40^\circ - 60^\circ$

Measured debond size range in cross-ply ( Correa et al., Compos. Sci. Technol. 155 (213-220), 2018 )

$21.4^\circ - 89.2^\circ$ , average  $49.3^\circ$ , standard deviation of  $11.7^\circ$   
63% of measurements in  $40^\circ - 60^\circ$  range

 **MOVING FORWARD**

## Moving Forward: Ideas

- ▶ Microscopic characterization of transverse cracks, debonds and microstructure: optical microscope and image analysis, edge view (both sides), increasing load levels on same specimen, different lay-ups and materials
  - SEM? TEM?  $\mu$ -CT?
- ▶ Microstructure-controlled debonding as toughening mechanisms for thin-ply laminates
  - 3D-printing? Improved spread-tow technique?

**Thank you for listening today!**



LULEÅ  
UNIVERSITY  
OF TECHNOLOGY



Education and Culture

Erasmus Mundus